Cell

# Dynein Motion Switches from Diffusive to Directed upon Cortical Anchoring

Vaishnavi Ananthanarayanan,[1] Martin Schattat,[1,3] Sven K. Vogel,[1,4] Alexander Krull,[1,5] Nenad Pavin,[1,2,*] and Iva M. Tolić-Nørrelykke[1,*]
[1]Max Planck Institute of Molecular Cell Biology and Genetics, 01307 Dresden, Germany
[2]Department of Physics, Faculty of Science, University of Zagreb, 10002 Zagreb, Croatia
[3]Present address: Department of Plant Physiology, Martin Luther University Halle-Wittenberg, 06120 Halle (Saale), Germany
[4]Present address: Max Planck Institute of Biochemistry, 82152 Martinsried, Germany
[5]Present address: Faculty of Computer Science, TU Dresden, 01187 Dresden, Germany
*Correspondence: npavin@phy.hr (N.P.), tolic@mpi-cbg.de (I.M.T.-N.)
http://dx.doi.org/10.1016/j.cell.2013.05.020

## SUMMARY

Cytoplasmic dynein is a motor protein that exerts force on microtubules. To generate force for the movement of large organelles, dynein needs to be anchored, with the anchoring sites being typically located at the cell cortex. However, the mechanism by which dyneins target sites where they can generate large collective forces is unknown. Here, we directly observe single dyneins during meiotic nuclear oscillations in fission yeast and identify the steps of the dynein binding process: from the cytoplasm to the microtubule and from the microtubule to cortical anchors. We observed that dyneins on the microtubule move either in a diffusive or directed manner, with the switch from diffusion to directed movement occurring upon binding of dynein to cortical anchors. This dual behavior of dynein on the microtubule, together with the two steps of binding, enables dyneins to self-organize into a spatial pattern needed for them to generate large collective forces.

## INTRODUCTION

Cytoplasmic dynein is a motor protein that walks along microtubules (MTs) and thereby moves organelles in the cell. Dynein uses MTs either as tracks to transport vesicles, proteins, and RNAs toward the cell center (Vallee et al., 2004) or as ropes to pull on structures such as the mitotic spindle (Eshel et al., 1993; Gönczy et al., 1999; Li et al., 1993; O'Connell and Wang, 2000; Skop and White, 1998), centrosome in interphase and in vitro (Burakov et al., 2003; Laan et al., 2012; Palazzo et al., 2001), and nucleus in meiotic prophase (Yamamoto et al., 1999). To pull on intracellular structures, dynein exerts force against anchor proteins fixed at the cell cortex (Burakov et al., 2003; Heil-Chapdelaine et al., 2000; Nguyen-Ngoc et al., 2007; Saito et al., 2006; Yamashita and Yamamoto, 2006) or against friction force generated by organelles as they move along the MT through the viscous cytoplasm (Kimura and Kimura, 2011). A central question is by which mechanism dyneins are targeted to sites where they can exert force.

A prominent example of a system where dynein anchored at the cortex drives large-scale movement by pulling on the MTs is nuclear oscillations in the fission yeast *Schizosaccharomyces pombe* (Yamamoto et al., 1999). The anchoring of dynein to the cell cortex occurs via the cortical anchor protein Num1/Mcp5 (Heil-Chapdelaine et al., 2000; Saito et al., 2006; Yamashita and Yamamoto, 2006). Nuclear oscillations occur during meiotic prophase and promote chromosome pairing, recombination and spore viability (Yamamoto et al., 1999). During the oscillations, the nucleus follows the spindle pole body (SPB; a centrosome equivalent in yeast), which moves back and forth from one cell end to the other. MTs grow from the SPB, with their minus ends at the SPB and plus ends pointing toward the cell periphery (Yamamoto et al., 1999). The mechanism of the oscillations relies on the asymmetric pattern of dyneins bound to a MT and the cortex, with more dyneins on the MT leading the SPB than on the MT trailing behind the SPB. This asymmetric pattern is a consequence of preferential unbinding of dynein from the trailing MT (Vogel et al., 2009). Hence, dyneins redistribute within the cell during each half-period of the oscillations to create such pattern. As they redistribute, dyneins need to find sites where they can bind to a MT and to cortical anchors in order to generate large collective forces.

Dynein binding from the MT to the cortical anchors has been studied in budding yeast, where dynein, anchored at the cortex, pulls on the MTs in order to move the mitotic spindle into the bud. As in fission yeast (Vogel et al., 2009), dynein appears first on astral MTs rather than on the cortex (Lee et al., 2003; Sheeman et al., 2003). However, unlike in fission yeast, dynein in budding yeast accumulates at the plus end of the growing MT in a Bik1/CLIP-170- and Pac1/LIS1-dependent manner, as a result of transport by the kinesin Kip2 or direct binding from the cytoplasm (Carvalho et al., 2004; Markus et al., 2009). When the plus end brings dynein close to the cortical anchors, dynein binds to the anchors in a process known as off-loading (Lee et al., 2003). Together, these studies have identified the molecular interactions of dynein necessary for cortical anchoring in budding yeast. However, the targeting mechanism of dynein to

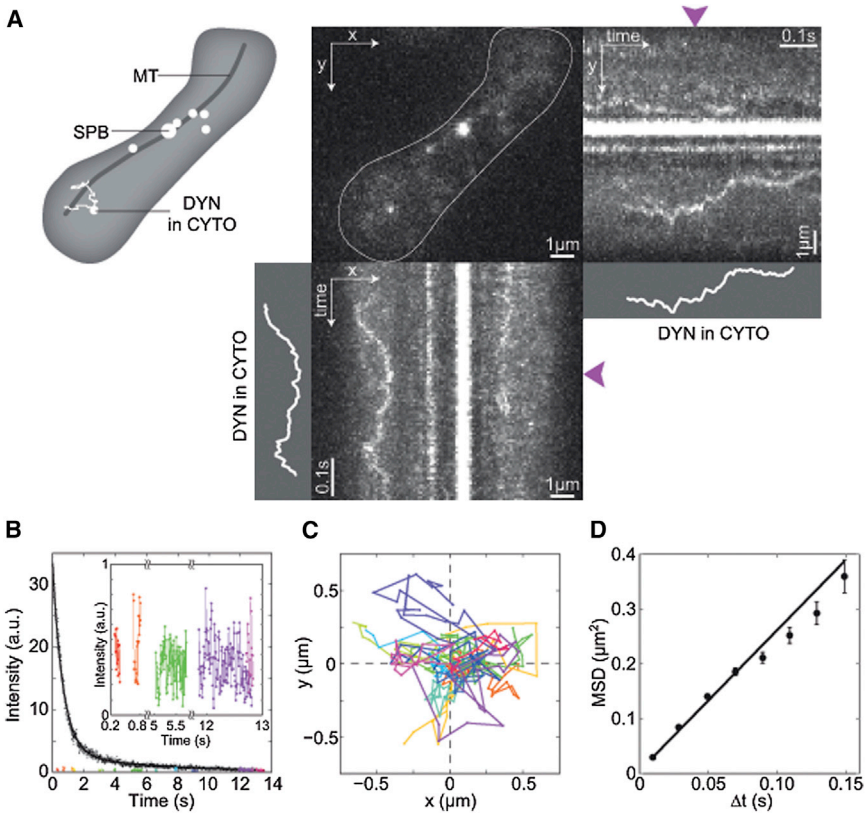


**Figure 1. Single Dyneins Diffuse in the Cytoplasm**

(A) Scheme (left) and HILO image (middle, Movie S1) of a fission yeast zygote expressing dynein heavy chain tagged with three GFPs (Dhc1-3GFP, strain SV56, Table S1). Dark gray lines in all schemes mark the approximate position of the microtubules in the imaged part of the cell. The white line in the image marks the cell outline. The movement of dyneins in the cytoplasm is visualized in consecutive maximum intensity projections onto the y axis (to the right of the image) and onto the x axis (below the image). The magenta arrowhead marks the time point of the HILO image. A trace of a dynein moving through the cytoplasm, obtained using the tracking software is shown in white ("DYN in CYTO").

(B) Intensity of dynein on the SPB (raw data shown by black circles and smoothed intensity obtained by the mean of every ten consecutive, nonoverlapping points, shown by the black line) and that of single dyneins in the cytoplasm in the same cell (n = 19, shown in different colors) expressing Dhc1-GFP (strain FY15548, Table S1). The inset shows the intensity of selected dyneins in the cytoplasm, indicating that their signal is similar throughout the movie.

(C) Traces of dyneins in the cytoplasm until a time of 0.14 s (n = 15 dyneins shown in different colors, strain SV56, Table S1).

(D) Mean-squared displacement (MSD) of dyneins in the cytoplasm as a function of time lag (black, error bars represent SEM, n = 443 dynein traces lasting for at least 60 ms from 104 cells of strain SV56, Table S1). A weighted fit to the equation $MSD = 4D_{cyt}\Delta t$ + offset (solid black line) yielded a diffusion coefficient $D_{cyt} = 0.64 \pm 0.01\ \mu m^2\ s^{-1}$ (mean ± SD).
See also Figure S1.

the cortical anchors at the single-molecule level is not known in any cell type.

Here, we investigate in fission yeast the mechanism by which dyneins target sites where they exert force. We set up the experiments to observe the movement of dyneins at the single-molecule level in vivo (Coelho et al., 2013). We were able to follow single dyneins on the MT and in the cytoplasm. Surprisingly, we were also able to directly visualize binding of dynein from the cytoplasm to the MT and to quantify this process. Direct single-molecule observations enabled us to discover a new property of dynein: although upon binding to the MT dynein moves in a diffusive manner, after binding to the cortical anchor it switches to directed movement and thus exerts force on the MT.

## RESULTS

### Direct Observation of Single Dyneins Diffusing in the Cytoplasm

We reasoned that if we could visualize the behavior of single dyneins in the cell, this would be a direct way to investigate the movement and kinetics of dynein. We first focused on dyneins in the cytoplasm, which are bound neither to a MT nor to the cortex. To this aim, we imaged fission yeast cells during meiotic prophase, in which all dynein motors were fluorescently labeled by tagging the dynein heavy chain with GFP (Vogel et al., 2009) (Dhc1-GFP; Table S1 available online). To detect single dyneins, we needed a high signal-to-background ratio, which we achieved by using highly inclined and laminated optical sheet microscopy (HILO) with a high laser power, on a total internal reflection fluorescence (TIRF) microscopy setup (Tokunaga et al., 2008) (Experimental Procedures). Whereas TIRF illuminates up to 200 nm from the surface of the coverslip, HILO allowed us to image deeper in the cytoplasm, up to a depth of 1.3 μm (Figure S1A). Because cytoplasmic diffusion is a fast process, we acquired images at the highest rate feasible in our setup: 200 frames/s (Experimental Procedures). We observed the appearance of bright particles at random times and locations in the cytoplasm and their movement in arbitrary directions (Figures 1A, S1B, and S1C; Movie S1).

In order to test whether the cytoplasmic particles represent single dynein motors, we quantified the signal intensity of the particles and of the dynein on the SPB, the brightest spot in the cell (Comparison of Intensity of SPB and Single Dynein in HILO). Each dynein motor is a dimer with two heavy chains, and thus carries two GFP molecules. We refer to dynein dimers simply as dyneins. The fluorescence of a visible dynein comes from either both GFPs, which is common at the beginning of imaging, or from only one GFP at later times, in case one GFP has been

photobleached during the imaging. Therefore, if the cytoplasmic particles represented a single dynein, we would expect the signal of particles appearing at the beginning of a movie to be up to twice the signal of those appearing later, regardless of the length of the movie. On the contrary, the signal of spots that contain a large number of GFPs decreases by order(s) of magnitude if the imaging time is longer than the decay time. We indeed observed that the signal of cytoplasmic particles decreased by <2-fold, whereas the signal of the SPB decreased 10-fold during the same time (Figure 1B). Consistently, we observed bleaching steps of dynein spots on the MT, with a step size similar to the intensity of a single GFP on dynein in the cytoplasm (Figure S1D). Additional evidence for the cytoplasmic particles being single dyneins is shown in Figures S1E–S1G. Taken together, these data indicate that we are observing single dyneins in the cytoplasm.

From movies of dynein diffusing in the cytoplasm, we estimated the total number of dyneins in the cytoplasm. We measured the number of dyneins in the illuminated part of the cytoplasm at the beginning of the movie, when bleaching can be neglected, to be 10 ± 3 dyneins (mean ± SD, n = 10 cells). Based on the size of the cell in our HILO images and the known geometry of the cell, we estimated that 1/3 ± 1/5 of the cell volume was illuminated (Figure S1A). Therefore, a typical cell contains approximately $n_{cyt}$ = 30 ± 20 (mean ± SD) dyneins in the cytoplasm, which corresponds to a concentration of $c$ = 0.3 ± 0.2 nM (mean ± SD) for a cylindrical cell with a volume of $V_{cell} = (2\ \mu m)^2 \times \pi \times 14\ \mu m \approx 180\ \mu m^3$.

To measure the diffusion coefficient of dynein in the cytoplasm, we tracked 443 dyneins from 104 cells (Figures 1A and 1C; tracking software is described in Experimental Procedures). In order to improve the signal-to-background ratio, we used a strain where the dynein heavy chain was tagged with three GFPs (Dhc1-3GFP) (Vogel et al., 2009), unless stated otherwise. As expected for diffusing particles, the mean-squared displacement of single dyneins scaled linearly with time, with a diffusion coefficient of 0.64 ± 0.01 $\mu m^2\ s^{-1}$ (mean ± SD, n = 443, Figure 1D; Tracking of Dyneins in the Cytoplasm). Similar results were obtained from cells expressing Dhc1-GFP (Figure S1H). An independent experiment using fluorescence recovery after photobleaching (FRAP) on cells overexpressing Dhc1-GFP (Spinning Disc Microscopy) yielded a diffusion coefficient of 0.6 ± 0.2 $\mu m^2\ s^{-1}$ (mean ± SD, n = 10 cells, Figure S1I). Similar diffusion coefficients obtained by these two different techniques suggest that the technique based on tracking single dyneins is reliable.

The diffusion of dynein is approximately ten times slower than the diffusion of GFP in the cytoplasm of *S. pombe* (Kalinina et al., 2013) and of *Escherichia coli* (Elowitz et al., 1999; English et al., 2011). Because dynein is approximately ten times larger in length than GFP (Johnson and Wall, 1983; Yang et al., 1996), the relationship between the diffusion and size of dynein and GFP is in agreement with the Einstein-Stokes equation, where the diffusion of a spherical particle in liquid scales inversely with the radius of the particle. With the diffusion coefficient measured here, dyneins require 2.5 min to spread from one end of a 14 μm long fission yeast zygote to the other. The period of nuclear oscillations is ~10 min (Chikashige et al., 1994), thus giving dynein sufficient time for redistribution by diffusion during a single period of oscillations.

## Single Dyneins from the Cytoplasm Bind to and Unbind from the Microtubule

Diffusion in the cytoplasm redistributes dynein throughout the cell, but to exert force on the MT dynein needs to be bound to the MT and to the cortex. Based on our previous observation that dynein unbinds from the cortex, but remains on the MT when the link between the MT and the cortex breaks (Vogel et al., 2009), we hypothesize that the binding of dynein occurs in two steps: (1) from the cytoplasm to the MT and (2) from the MT to the cortex.

If we could visualize binding events of single dyneins, such as binding from the cytoplasm to a MT and from the MT to the cortex, these experiments would directly uncover the binding process of dynein. MTs in these cells are organized in two to three bundles, each consisting of one to ten MTs (Vogel et al., 2009). MTs in a bundle move neither with respect to the SPB nor with respect to one another (Yamamoto et al., 2001), thus we refer to MT bundles simply as MTs. We identified MTs by drawing a line through the stationary signal of dynein (Figure 2A) because MTs are decorated with dyneins (Vogel et al., 2009). Indeed, cells with mCherry-tagged MTs and GFP-tagged dynein showed dynein spots along the MTs (Figure S2A). In our HILO experiments, we observed events when the pronounced movement of a dynein stopped abruptly (Figure 2A; Movie S2). In all the observed events, dynein movement stopped at a location that corresponded to the MT (n = 27/27 events from 104 movies, Figure S2B; Estimation of Binding Events). These data show that dynein from the cytoplasm typically binds to a MT, as opposed to binding to cortical regions devoid of MTs. We also observed reverse events (n = 6) where dynein was first stationary and then started diffusing (Figures 2B and S2C; Movie S3). Thus we conclude that dynein in the cytoplasm can bind to and unbind from the MT.

From the observed binding events, we calculate the binding rate of dynein to the MT as the ratio of the number of binding events to the total duration of traces of all dyneins visible in the cytoplasm (Figure S2D), $k_{on} = (27 \pm \sqrt{27})/1{,}440\ s^{-1} = 0.019 \pm 0.004\ s^{-1}$ (mean ± SD). The calculated binding rate implies that a dynein motor typically spends $1/k_{on}$ = 53 s in the cytoplasm before binding to a MT.

## Dyneins Diffuse along the Microtubule upon Binding from the Cytoplasm

We have observed single dynein motors from the cytoplasm binding to the MT. These measurements, however, do not show whether these dyneins are also bound to the cortex, which is necessary for them to pull on the MT. We now consider dyneins on the leading MT because these are the ones that exert the pulling forces that drive nuclear movement. The leading MT is decorated with dyneins (Figure 3A) and in this crowded environment, tracking of single dyneins is unreliable. Therefore, we first photobleached the GFPs on dyneins in the whole field of view by taking a HILO movie as before, so that at the end of the movie, the GFPs in the plane illuminated by HILO were bleached, whereas those in the nonilluminated part of the cell remained unbleached (Figure 3B; Experimental Procedures). Subsequently, we took a second movie with the image acquisition rate reduced to 1 frame/s (Figure 3C) in order to observe dyneins

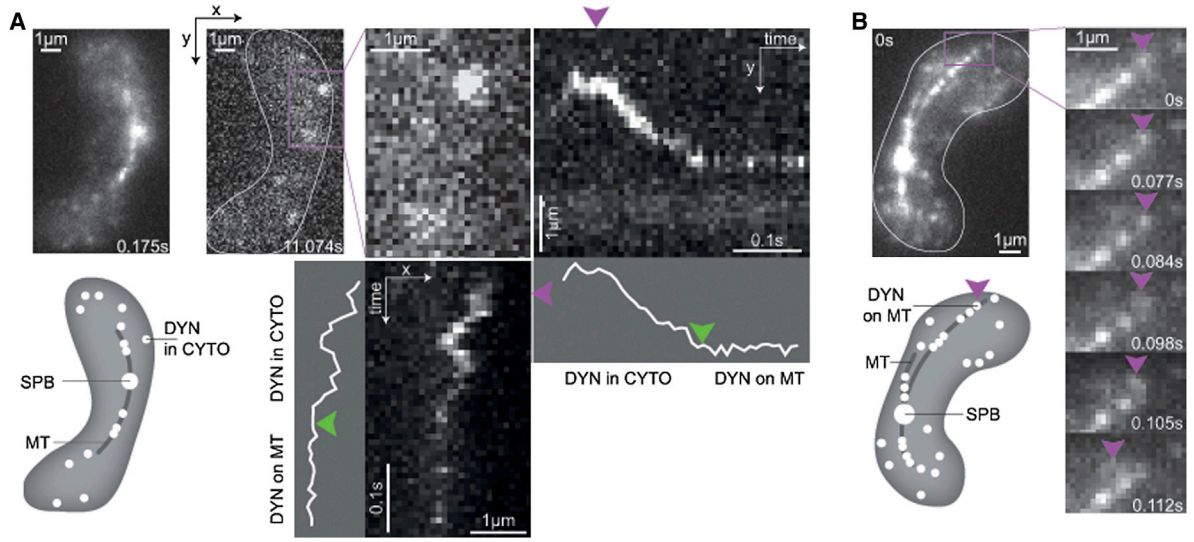


**Figure 2. A Dynein from the Cytoplasm Binds to and Unbinds from the MT**

(A) Binding event. An image from the beginning of the movie, from which the position of the MT is inferred and the corresponding scheme (below). The cell at a later time when the dynein molecule of interest appears (second from the left, Movie S2); the white line marks the cell outline. The enlarged view of the area inside the magenta rectangle with the dynein of interest (third image from the left) and consecutive maximum intensity projections onto the y axis (to the right of the image) and onto the x axis (below the image). The projections show the dynein moving through the cytoplasm ("DYN in CYTO") and later binding to the MT (green arrowheads, "DYN on MT"). The trace of the dynein obtained using the tracking software is shown in white. The magenta arrowheads mark the time point of the HILO image with the dynein of interest.

(B) Unbinding event. Image of the cell (left) and the corresponding scheme (below) at t = 0, when the dynein of interest (magenta arrowhead) is bound to the MT. The white line marks the cell outline. The panel on the right is a time-lapse sequence of the area marked by the magenta rectangle and shows the unbinding of the dynein (magenta arrowheads, Movie S3) from the MT into the cytoplasm. In (A) and (B), cells expressing Dhc1-3GFP (strain SV56, Table S1) were imaged using HILO microscopy.

See also Figure S2.

on a timescale relevant for SPB movement (tens of seconds) and before their signal disappeared due to bleaching (bleaching time ~150 s, see Figure 1B). In this movie, we were able to observe abrupt appearance of dynein on the MT, which we interpret as binding of a single dynein from the cytoplasm to the MT (Figure 3C; Movie S4; an example with labeled MTs is shown in Figure S3A). These dyneins moved with respect to the cell cortex, suggesting they were not bound to the cortex but only to the MT (Figure 3C). We confirmed that these events represent single dyneins by comparing their signal intensity with that of single dyneins in the cytoplasm (Figure S3B). Thus, we use abrupt appearance of signal on the MT as a criterion for identification of dynein binding to the MT from the cytoplasm.

We asked whether dyneins on the MT move in a directed manner and if so, toward which end of the MT. We observed that the traces representing single dyneins riding on the MT were roughly parallel to the trace of the SPB (Figure 3C). This observation indicates that dyneins did not move in a directed manner along the MT toward either MT end. This conclusion was based on the fact that the MT lattice moves together with the SPB, because minus ends of all MTs are at the SPB and do not exhibit dynamics (Yamamoto et al., 2001). To test whether this behavior is typical for dynein that is not bound to the cortex, we deleted the cortical anchor Mcp5/Num1. In the absence of cortical anchors (*mcp5/num1*Δ), the SPB oscillations vanished, whereas the traces of dyneins on the MT remained roughly parallel to the trace of the SPB (Figure 3D). Thus, dyneins that are bound only to the MT do not move in a directed manner.

To quantify the movement of single dyneins along the MT, we tracked all dyneins that bound to and remained on the MT for more than 10 s in wild-type and in a *mcp5/num1*Δ strain. Dynein positions were measured relative to the SPB. A linear relationship between mean squared displacement and time showed that dynein movement with respect to the MT was diffusive in both cases. The diffusion coefficient of dynein in wild-type was similar to that in *mcp5/num1*Δ, 0.0041 ± 0.0007 $\mu m^2\ s^{-1}$ and 0.0050 ± 0.0003 $\mu m^2\ s^{-1}$, respectively (mean ± SD, n = 49 in wild-type and 39 in *mcp5/num1*Δ; Figure 3E). When compared to the movement of dynein in the direction parallel to the MT, the movement perpendicular to the MT was negligible (Figure S3C). We conclude that diffusion along the MT is the default behavior of dynein bound only to the MT.

The signal of the dyneins on the MT disappeared abruptly (Figure 3C), which could have been due to dynein unbinding from the MT or photobleaching. We calculate $k_{off}$ as the ratio of the number of dynein disappearances to the total signal duration of all dyneins that bound to the leading MT and lasted for at least 3 s, $k_{off} = (74 \pm \sqrt{74})/840\ s^{-1} = 0.09 \pm 0.01\ s^{-1}$ (mean ± SD). This rate was 10 times larger than the rate of photobleaching, where the latter was inferred from the decay of the dynein-3GFP signal on the SPB (0.007/frame at 135 frames/s, n = 10 cells). Therefore, as photobleaching can be neglected,

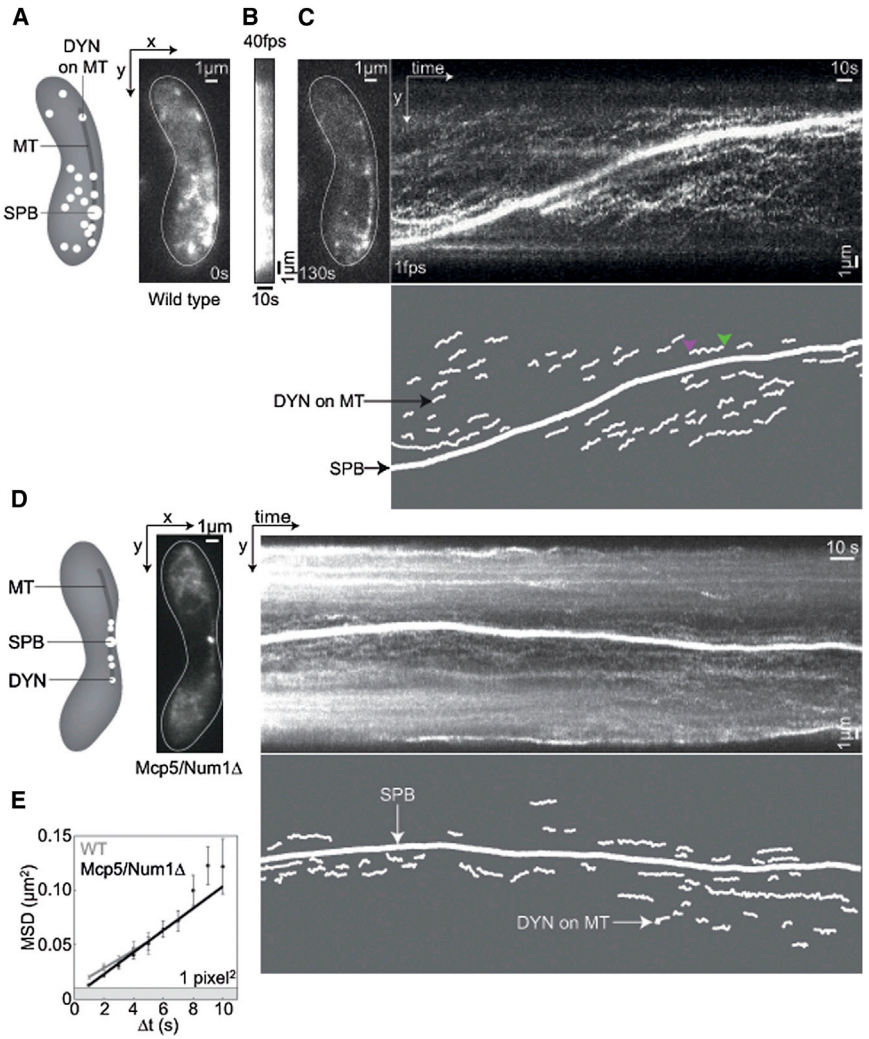


**Figure 3. Dyneins Diffuse along the MT upon Binding from the Cytoplasm**

(A) Scheme of the cell (left) and a HILO image of the green channel showing dynein at t = 0 (right) in a cell expressing Dhc1-GFP and Mcp5/Num1-tdTomato (strain SV93, Table S1; Construction of Strains, Plasmid Transformation, Meiosis Induction and Preparation of Cells for Imaging). The white line marks the cell outline.

(B) Dynein was first bleached by taking a movie at 40 frames/s. Consecutive maximum intensity projections onto the y axis are shown.

(C) Green channel showing dynein after the frame rate was reduced to 1 frame/s (Movie S4). The movement of dyneins on the MT is visualized in consecutive maximum intensity projections onto the y axis (to the right of the image). The traces of dyneins that appeared on the MT and the trace of the SPB are shown below. The arrowheads mark an example of dynein signal appearing (magenta) on the MT and disappearing (green). In this movie, there were 1.9 ± 1.8 (mean ± SD) visible dyneins diffusing along the MT at any given time after the bleaching shown in (B).

(D) Dynein diffuses on the MT in a *mcp5/num1Δ* strain. Scheme (left) and image (center, obtained using HILO microscopy) of a cell in which dyneins are labeled with 3GFP and the anchors have been deleted (*mcp5/num1Δ*, Dhc1-3GFP, strain JT932, see Table S1). On the top right is the maximum intensity projection onto the y axis of the cell along time. On the bottom right are the traces obtained upon tracking all the dyneins that appeared on the MT. The dynein traces here are also roughly parallel to that of the SPB, similar to the wild-type dynein traces.

(E) Mean-squared displacement (MSD) of dyneins with respect to the MT as a function of time lag (error bars represent SEM, n = 49 dynein traces lasting for at least 9 s from 20 cells from strain SV81). Dynein positions were measured relative to the SPB. A weighted fit to the equation $MSD = 2D_{MT}\Delta t$ + offset (gray line) yielded a diffusion coefficient $D_{MT} = 0.0041 \pm 0.0007\ \mu m^2\ s^{-1}$ (mean ± SD). For the *mcp5/num1Δ* strain, a weighted fit to the equation $MSD = 2D_{MT}\Delta t$ + offset (black line) yielded a diffusion coefficient $D_{MT} = 0.0050 \pm 0.0003\ \mu m^2\ s^{-1}$. Grey denotes the area where the data corresponding to subpixel movement of dynein would be found. See also Figure S3.

$k_{off}$ reflects the rate of dynein unbinding from the MT, implying that dynein typically stays on the MT for $\tau = 1/k_{off} = 11 \pm 1$ s (mean ± SD).

## Dyneins on the Microtubule Are Activated as Minus-End-Directed Motors upon Binding to Cortical Anchors

To generate force on the MT, dynein needs to be bound to the MT and to the cortical anchor Mcp5/Num1 (Saito et al., 2006; Yamashita and Yamamoto, 2006). We have shown that dynein from the cytoplasm binds to the MT (Figure 2A), but not simultaneously to the cortex (Figure 3C). Does this dynein subsequently bind to the cortex? In our HILO experiments, we identified cortically anchored dyneins as spots that did not move with respect to the cell cortex. These stationary dyneins colocalized with Mcp5/Num1 (Saito et al., 2006) in a strain expressing Dhc1-GFP and Mcp5/Num1-tdTomato (Figure S4A), suggesting that they were indeed anchored at the cortex.

The signal of spots of anchored dyneins typically increased in time (Vogel et al., 2009) (Figure 4A), corresponding to an increase in the number of anchored dyneins at the same site. A few seconds before the increase, we typically observed binding of a new dynein to the MT in the neighborhood of the anchored dyneins (Figure 4A; Movie S5; see also four other such events in Figure S4B). The subsequent increase in the signal of anchored dyneins was accompanied by a decrease in the signal in the neighborhood (17 out of 20 events in six cells, Figures 4A and S4C). We interpret this change in the dynein signal along the MT from a broad profile into a peaked one as anchoring of a new dynein from the MT to the cortex. These data imply that cells would have fewer anchored dyneins if MTs were absent. Indeed, we observed that by depolymerizing MTs using a MT inhibitor MBC (MBC Experiments), we abolished the localization of dynein to the cortical anchors (Figure S4D). We conclude that dyneins target cortical anchors primarily by binding first from

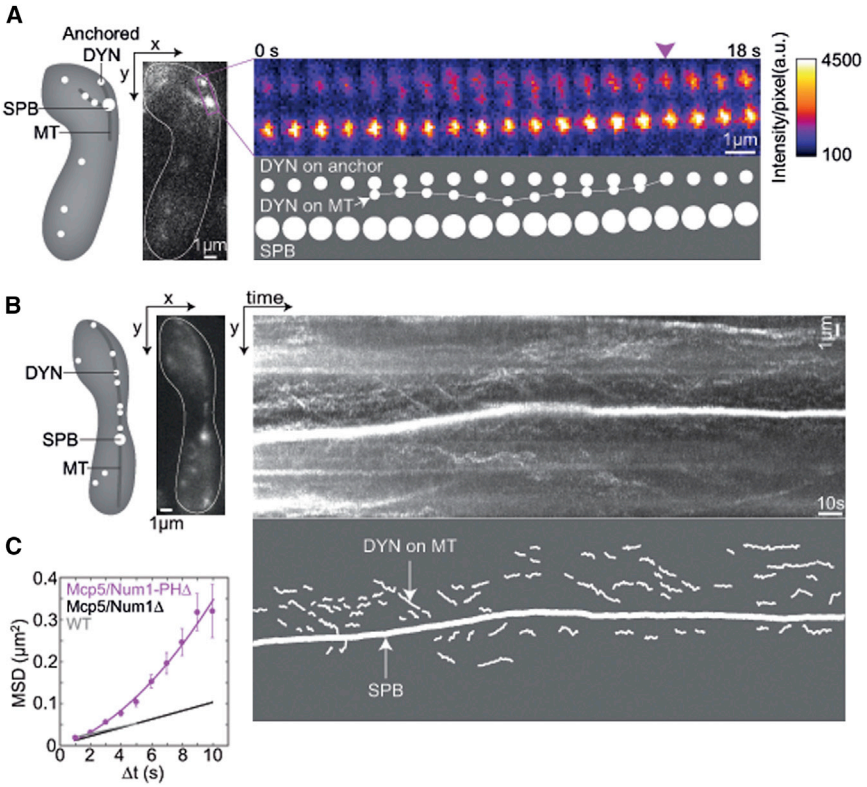


**Figure 4. Dyneins on the MT Become Activated upon Binding to the Anchor Protein Mcp5/Num1**

(A) Scheme (left) and image (middle, obtained using HILO microscopy) of a cell expressing Dhc1-3GFP and mCherry-α2-tubulin (strain SV81, Table S1). Time-lapse sequence of images (right) showing the area marked by the magenta rectangle. The images and the schemes below show anchored dynein ("DYN on anchor"), dynein moving along the MT ("DYN on MT"), and dynein on the SPB. The color scale indicates the intensity per pixel, with black denoting 100 a.u./pixel and white denoting 4,500 a.u./pixel. The dynein that moved along the MT stopped moving at the location of the anchored dynein (magenta arrowhead, Movie S5). Consequently, the intensity of anchored dynein ("DYN on anchor") moves up on the color scale.

(B) Scheme (left) and image of a cell (middle, obtained using HILO microscopy) of a cell expressing Dhc1-3GFP and the anchor Mcp5/Num1 with its PH-domain deleted (*mcp5/num1-PHΔ*, strain JT932 transformed with plasmid p3CH1-num1PHΔ, Table S1). Maximum intensity projections onto the y axis (right, top) and the corresponding traces of dynein that appeared on the MT (right, bottom). In contrast to Figure 3C, dyneins exhibiting directed movement toward the SPB can be seen (Movie S6). Note that the SPB does not move as much as in wild-type.

(C) Mean-squared displacement (MSD) of dyneins with respect to the MT as a function of time lag in the *mcp5/num1-PHΔ* strain (magenta, error bars represent SEM, n = 52 dynein traces lasting for at least 20 s from 14 cells from strain JT932 transformed with plasmid p3CH1-numPHΔ). Dynein positions were measured relative to the SPB. For the *mcp5/num1-PHΔ* strain, a fit to the equation $MSD = v^2\Delta t^2 + 2D_{MT}\Delta t +$ offset (magenta line) yielded a velocity $v = 2.8 \pm 1.0$ μm/min and diffusion coefficient $D_{MT} = 0.006 \pm 0.008$ μm$^2$ s$^{-1}$. The obtained velocity is most likely smaller than the velocity of the processive movement of dynein, because the data include all dyneins on the MT and thus also those that were not bound to the truncated anchor Mcp5/num1-PHΔ. The black and gray lines show the MSD fit for *mcp5/num1Δ* and wild-type, respectively, from Figure 3E for comparison. We are showing a quadratic fit for the *mcp5/num1-PHΔ* strain because the quadratic formula fits better the data ($r^2 = 0.99$ and 0.95 for the quadratic and linear fit, respectively).

See also Figure S4.

the cytoplasm to the MT and then to the anchors, as opposed to binding from the cytoplasm directly to the anchors.

We next asked whether dynein switches from diffusive to directed motion toward the minus end of the MT upon anchoring to the cell cortex. We refer to this switch as activation of dynein. The anchored dyneins were stationary with respect to the cell cortex, whereas the SPB and thus the minus end of the MT (Yamamoto et al., 2001) moved toward these dyneins (Figure 4A). Because the anchored dyneins remained in the close proximity to the MT, we conclude that these dyneins moved in a directed manner along the MT toward the minus end, contrary to the nonanchored dyneins on the MT, which moved in a diffusive manner.

Is binding of dynein to the cortical anchor sufficient for dynein activation? If this were the case, then a cell with truncated anchors, which can bind to dynein but not to the cortex, would show dyneins moving in a directed manner along the MT toward the minus end, instead of diffusing along the MT as in wild-type. To test this hypothesis, we abolished the ability of the anchor to bind to the cell cortex by deleting the anchor's pleckstrin-homology (PH) domain (Saito et al., 2006; Yamashita and Yamamoto, 2006) (*mcp5/num1-PHΔ*, see Experimental Procedures and Table S1). First, we expressed Mcp5/num1-PHΔ in a strain where Mcp5/Num1 was deleted and dynein heavy chain was tagged with 3GFP. In this strain, we observed dyneins that move in a directed fashion toward the minus end of the MT, in addition to the diffusing dyneins on the MT (Figure 4B; Movie S6; see also Figure S4E for more examples). This behavior is in contrast to that of nonanchored dyneins in wild-type and in a *mcp5/num1Δ* strain, where dyneins on the MT are only diffusive (Figures 3C and 3D), showing that dynein becomes active as a minus-end-directed motor in the presence of Mcp5/num1-PHΔ. Second, we expressed Mcp5/num1-PHΔ-GFP from a plasmid in a strain where dynein heavy chain was tagged with tdTomato. In contrast to wild-type, this strain showed a strong signal of Mcp5/num1-PHΔ-GFP on the SPB, which suggests an interaction between Mcp5/num1-PHΔ and dynein on the SPB (Figure S4F). Note that the SPB oscillations were similar to those in wild-type because of the presence of native Mcp5/Num1 in this strain. Similar to the first case, we observed dyneins that move in a directed manner toward the minus end of the MT (Figure S4G). These results suggest that binding of dynein to the cortical anchor activates dynein as a minus end-directed motor.

**Table 1. Measured Parameters Related to Dynein Redistribution within the Cell**

| Parameter | Description | Value |
|---|---|---|
| $D_{cyt}$ | diffusion coefficient of dynein in the cytoplasm | $0.64 \pm 0.01\ \mu m^2\ s^{-1}$ |
| $k_{on}$ | binding rate of dynein to MT (direct observation, estimated by the model) | $0.019 \pm 0.004\ s^{-1}$, $0.07 \pm 0.05\ s^{-1}$ |
| $k_{off}$ | unbinding rate of dynein from the MT | $0.09 \pm 0.01\ s^{-1}$ |
| $\tau$ | dwell time of dynein on the MT, $\tau = 1/k_{off}$ | $11 \pm 1$ s |
| $D_{MT}$ | diffusion coefficient of dynein along the MT | $0.0041 \pm 0.0007\ \mu m^2\ s^{-1}$ |
| $k_a$ | binding rate of dynein from the MT to cortical anchors (estimated by the model) | $0.1\ s^{-1}$ |
| $k_u$ | unbinding rate of dynein from cortical anchors to MT (depends on the load) | variable |
| $n_{cyt}$ | number of dyneins in the cytoplasm | $30 \pm 20$ |
| $n_{SPB}$ | number of dyneins on the SPB | $152 \pm 139$ |
| $n_{MT}$ | number of dyneins on the MT | $1.6 \pm 0.4\ \mu m^{-1}$ |
| $n_a$ | number of dyneins on an anchor | $28 \pm 8$ |
| $c$ | dynein concentration in the cytoplasm, $c = n_{cyt}/V_{cell}$ | $0.3 \pm 0.2$ nM |

We next quantified the movement of dyneins in the strain expressing Mcp5/num1-PHΔ and Dhc1-3GFP described above. Mean-squared displacement of dyneins on the MT showed a parabolic dependence on time, revealing that these dyneins perform directed movement (Figure 4C). This movement is in contrast to the movement of dyneins in the *mcp5/num1*Δ strain and of nonanchored dyneins in wild-type, which move in a diffusive manner (Figures 3E and 4C). MT dynamics in the *mcp5/num1-PH*Δ and *mcp5/num1*Δ strains were similar (Figure S4H; Table S2) and thus cannot account for the difference in dynein behavior in the two strains. In the *mcp5/num1-PH*Δ strain, we used kymographs to estimate a velocity of 8.3 ± 0.8 μm/min of those dyneins that exhibited directed movement (n = 52 traces; Figures S4E and S4I). This velocity is similar to the velocity of budding yeast dynein heavy chain in vitro (Reck-Peterson et al., 2006). We estimated that 25% of the dyneins on the MT moved in a directed manner (29 out of 122; the estimation we used is described in Figure S4I). Taken together, these results show that dyneins bound only to the MT are inactive, becoming activated upon binding to the anchor.

## Parameters of Dynein Dynamics Relevant for SPB Oscillations

To complete the picture, we performed the total count of dyneins at different locations in the cell. We measured roughly 100 dyneins on the SPB, which may include dyneins bound to short MTs, with a length below the resolution of the microscope, in the vicinity of the SPB (Figure S1E). The brightest spot of dyneins bound to the MT and anchored at the cortex contains roughly 30 dyneins (Figure S5A), which is comparable to the number of anchored dyneins in budding yeast (Markus et al., 2009). Typically two to three spots of similar or smaller intensity are formed during a half-period of nuclear oscillations. We estimated ~23 dyneins diffusing along a 14 μm-long MT at any given time ($n_{MT} = 1.6 \pm 0.4\ \mu m^{-1}$, mean ± SD, n = 15 cells; Estimation of Number of Dyneins Diffusing along the MT) and, as mentioned above, we measured $n_{cyt} = 30$ dyneins in the cytoplasm. Thus, there are ~200 dynein molecules in a fission yeast cell during meiotic prophase.

The measured number of dyneins in the cytoplasm and on the MT, and the binding and unbinding rates of the two-step binding process are mutually dependent. We now re-evaluate the binding rate of dynein from the cytoplasm to the MT, $k_{on}$, by using other measured parameters. We consider the trailing MT, where the density of dyneins bound only to the MT is a result of binding of dynein from the cytoplasm to the MT and the reverse process. This situation corresponds to a steady state solution of the two-step model from Vogel et al. (2009), which is described in The Model (Equations 3 and 4), giving

$$k_{on} = \frac{k_{off}\, n_{MT} L_{cell}}{n_{cyt}} = 0.07 \pm 0.05\ s^{-1}.$$

This rate is larger than $k_{on} = 0.019 \pm 0.004\ s^{-1}$, which was measured directly. The rate obtained by direct observations was most likely underestimated because binding events, which were identified as the moment when the movement of a dynein in the cytoplasm stops (Figure 2A), were hard to observe in the beginning of the movie when the MT was decorated with numerous unbleached dyneins (Figure S2B).

Finally, we estimate the effective binding rate of dynein from the MT to the cortical anchors, $k_a$, which represents the rate of binding of dynein from the MT to an arbitrary position along the cortex. Note that in this calculation we assume a homogeneous distribution of anchor proteins, as in Vogel et al. (2009), rather than an inhomogeneous distribution, which is observed experimentally (Figure S4A). To estimate this rate, we compare the measured number of dyneins on the leading MT with the corresponding numbers of dyneins obtained by the model (Figures S5B–S5K). We find that for $k_a = 0.1\ s^{-1}$, by using the values of $k_{on}$, $k_{off}$ and $c$ measured here, the number of dyneins obtained by the model is comparable to the values measured in our experiments. For these parameters, the pattern of oscillations is consistent with the experimentally observed oscillations (Vogel et al., 2009). Thus, our new measurements provide support for our previous model of nuclear oscillations.

The parameters relevant for nuclear oscillations are summarized in Table 1. Taken together, our data show that the two-step binding process, from the cytoplasm via the MT to

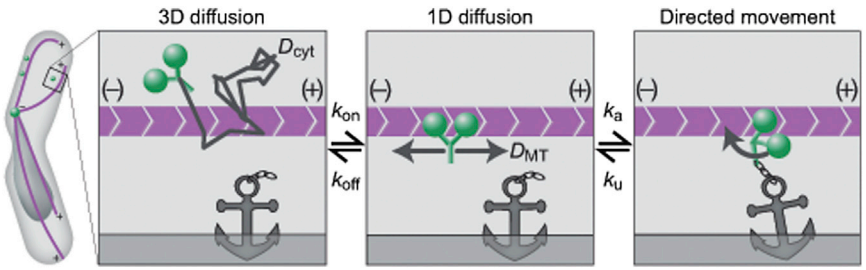


**Figure 5. Two-Step Process of Dynein Binding to the MT and Cortical Anchors**

Scheme of the cell (first from left) and an enlarged region where a MT is close to the cell cortex (area marked by the black rectangle). The subsequent panels illustrate the key steps in the binding and unbinding of dynein. Dynein (green) diffuses in the cytoplasm, binds to and unbinds from the MT (magenta; first panel). Once on the MT, dynein performs one-dimensional diffusion along the MT (second panel). When dynein gets close to a cortical anchor, it binds to the anchor (third panel; please note that this interaction is most likely indirect). Upon binding to the anchor, dynein starts to walk toward the minus end of the MT, thereby pulling on the MT. See also Figure S5.

the anchors, allows dyneins to target sites where they can exert forces responsible for large-scale nuclear movements (Figure 5).

## DISCUSSION

### Direct Observation of Single Dyneins as They Move through the Cell

Observation of single dyneins diffusing in the cytoplasm and along the MT allowed us to identify key steps of the redistribution of dynein within the cell, binding from the cytoplasm to the MT and from the MT to the cortical anchors, as well as the reverse steps. Importantly, it allowed us to quantify the motion of dynein in the cytoplasm and along the MT, as well as the kinetics of this reaction-diffusion process. These measurements were possible because of a high signal-to-background ratio and a high speed of imaging. It would be interesting, for example, to use this approach on kinesin-1 in mammalian cells or dynein in *Ustilago*, as single motors have already been observed as they move along MTs in those systems (Cai et al., 2007; Schuster et al., 2011).

### How Motors Find Sites Where They Can Exert Force: Two-Step Binding Process of Dynein

To exert forces, motor proteins bind with their head domain to a cytoskeletal filament and with their tail domain to another object, such as cell cortex, a vesicle, or a tail domain of another motor. A general question is how motors search for sites in the cell where both these domains can bind to their respective binding partners.

Here, we have shown that dynein during meiotic prophase in fission yeast binds in two steps, first from the cytoplasm to the MT and then also to the cortical anchor (Figure 5). Similar to the second step observed here, MTs deliver dynein to the cortex in budding yeast (Lee et al., 2003; Sheeman et al., 2003). Future studies will reveal the first step, namely, how dynein binds to the MT in that system.

What is the advantage of dynein binding to the MT first, as opposed to a hypothetical scenario where it binds to the anchor first? If dyneins bound to the anchors first, they would have to wait for a MT to reach them, because anchors are stationary. However, this would be an inefficient strategy because the MT does not explore the cortex by moving laterally and thus is in the vicinity of only a small number of anchors. This would leave dyneins bound to all the other anchors unable to bind to the MT. On the contrary, when dyneins bind to the MT first, they move with respect to the cell cortex by the gliding of the MT and by their movement along the MT. Thus they explore the cortex and eventually find an anchor.

### Dual Behavior of Dynein on the Microtubule: A Switch from Diffusion to Directed Movement

We found that dynein either diffuses along the MT or moves in a directed manner toward the minus end of the MT. The switch from diffusion to directed movement occurs upon binding of dynein to a cortical anchor (Figure 5). This dual behavior of dynein is surprising, because dynein is regarded as a minus end-directed motor (Paschal and Vallee, 1987; Reck-Peterson et al., 2006).

What is the mechanism underlying the switch between directed and diffusive motion of dynein? A possible scenario is inhibition of the motor activity by the interaction between the head and the tail domain of the motor protein, as found in vitro for kinesin-1 (Coy et al., 1999; Friedman and Vale, 1999; Hackney et al., 1992), kinesin-2 KIF17 (Hammond et al., 2010), kinesin-3 KIF1A (Hammond et al., 2009), and myosin V (Krementsov et al., 2004; Li et al., 2004; Wang et al., 2004). For kinesin-1, this inhibition was inferred from the observed decrease in the motor velocity and frequent pausing (Friedman and Vale, 1999). It was suggested that in cells, the motor activity is regulated by binding of cargo to the tail domain, which disables the interaction between the head and tail domain, thereby allowing the motor to perform its function of transport inside the cell (Coy et al., 1999; Friedman and Vale, 1999; Hackney et al., 1992).

A similar regulation of activity may also be a property of dynein. Single dyneins have been shown to move processively toward the minus end of the MT in vitro (Mallik et al., 2004; Reck-Peterson et al., 2006; Toba et al., 2006), although bidirectional and diffusive motion has also been observed (Ross et al., 2006; Trokter et al., 2012). In budding yeast, it has been shown that dynein is active, moving processively toward the minus end of the MT, or inactive. The activation occurs upon binding of dynein to the cortical anchor (Lee et al., 2003; Sheeman et al., 2003). In addition, it has been suggested that the tail domain is masked by the head domain, whereas unmasking occurs upon targeting of dynein to the MT plus end, based on the observation that dynein mutants with a peptide inserted between the anchor-binding tail and the MT-binding head

domain exhibit enhanced binding to cortical anchors (Markus and Lee, 2011; Markus et al., 2009). In fission yeast, however, dynein binds the cortex from the lateral side of the MT, rather than specifically from the plus end (Vogel et al., 2009). Moreover, we have shown here that the fission yeast dynein switches from diffusion to directed motion, which has not been observed in budding yeast. Further studies will identify the accessory proteins relevant for the different modes of dynein motion and the switch from one mode to the other in different organisms.

What could the benefit of the dual behavior of dynein be? We speculate that if dynein did not show dual behavior, but instead always moved in a directed manner toward the minus end of the MT, this property of dynein would result in a less efficient mechanism to generate nuclear oscillations. In this case, all dyneins bound to the MT, irrespective of whether they are also bound to the cortex or not, would move with similar velocities (Vogel et al., 2009). Therefore, all the dyneins bound to the MT would be stationary with respect to the cell cortex. Consequently, dyneins that are bound only to the MT would not be able to explore the cortex in search for anchors. On the contrary, dual behavior of dynein may allow it to explore the cortex, by being passively transported by the sliding movement of the MT and by diffusing along the MT.

Several other motor proteins and other MT-associated proteins have been observed to diffuse along MTs (Cooper and Wordeman, 2009). The diffusion coefficient of dynein measured in this work was one to two orders of magnitude lower than that of MCAK, myosin Va, Ase1, XMAP215, Dam1, and Ndc80 measured on MTs in vitro (Ali et al., 2007; Brouhard et al., 2008; Gestaut et al., 2008; Helenius et al., 2006; Kapitein et al., 2008; Powers et al., 2009). Further work will reveal whether this difference results from different conditions in vivo and in vitro, or from different mechanisms of diffusion between various motors and other MT-associated proteins.

In conclusion, observation of single dyneins in the cytoplasm and on the MT enabled us to reveal the mechanism by which dyneins target sites where they can bind to a MT and to cortical anchors. We have shown that dynein binds in two steps, the first step being binding from the cytoplasm to the MT. Once on the MT, dynein performs one-dimensional diffusion along the MT, but switches to directed motion upon binding to a cortical anchor. These properties of dynein, unveiled by direct observation of single molecules in vivo, constitute the mechanism by which dyneins find cortical anchors in order to generate large-scale movements in the cell.

## EXPERIMENTAL PROCEDURES

### Strains and Media

Fission yeast strains used in this study are listed in Table S1. Cells were grown on yeast extract (YE) or Edinburgh minimal medium (EMM) (Forsburg and Rhind, 2006) with appropriate supplements at 25 ± 0.5°C in a Heraeus incubator (Thermo Scientific). For inducing meiosis, cells were spotted on malt extract agar (MEA) plates.

### Construction of Strains, Plasmid Transformation, Meiosis Induction, and Preparation of Cells for Imaging

Construction of strains SV93 and SV108 (Table S1), transformation of strains JT392 and FY16826 (Table S1) using lithium acetate and the general protocols used for induction of meiosis and preparation of cells for imaging are described in Extended Experimental Procedures.

### Highly Inclined and Laminated Optical Sheet Microscopy

An inverted stand, manual XY stage Olympus IX71 microscope (Olympus) with custom-built TIRF condenser and manual TIRF angle adjustment was employed. Imaging was performed using an Olympus UApo 150× 1.45 Oil TIRFM inf/0.13-0.21 corr (Olympus) objective with diode-pumped solid state 491 nm laser for GFP excitation and 560 nm laser for mCherry/tdTomato excitation (75 mW; Cobolt). Laser intensity was controlled using the acousto-optic tunable filter in the Andor Revolution laser combiner (ALC; Andor Technology). The wavelength filters used were the BL HC 525/30 for GFP emission and the BL HC 607/36 for mCherry/tdTomato emission (Semrock). The microscope was equipped with an Andor iXon EM+ DU-897 BV back illuminated EMCCD (Andor Technology) with pixel size of EMCCD chip being 16 μm and image pixel size being 0.106 μm with the 150× objective. The system was controlled using the Andor iQ software version 1.9.1 (Andor Technology).

For imaging dynein in the cytoplasm (Figures 1 and 2; Movie S7), the imaging conditions used were: excitation with 80% power (18 mW) of 491 nm laser, exposure time of 5–9 ms, with 2,000 continuous repetitions. For imaging dynein on the MT (Figures 3 and 4), the zygotes were first subjected to 80% power (18 mW) of 491 nm laser, exposure time of 8 ms, with 800 continuous repetitions. This procedure partially bleached the dyneins on the MT. Subsequently, the zygotes were imaged sequentially with 80% power (18 mW) of 491 nm laser and 20% power (4 mW) of 560 nm laser, exposure time of 8 ms each, with an interval of 1 s between each sequential set, repeated 500 times. An exception was Figure 3C, where repeated imaging with the 560 nm laser was replaced by a single image taken with that laser.

### Image and Data Analysis

To track dyneins, we used a maximum likelihood method to automatically extract the positions of dyneins from the acquired movies. Methods of this kind (Abraham et al., 2009) have been shown to achieve a higher precision compared to the more widely used least-squares fit approaches. We assumed the intensity of each pixel in an image to follow a Poisson distribution. The mean value of each pixel is modeled as a sum of a Gaussian function of its position and a constant value, representing a dynein and the background, respectively. We used an Expectation Maximization algorithm to estimate the following parameters: position, SD, intensity of dynein, as well as the mean background intensity. The details of this method will be published elsewhere. Mean squared displacement analysis was performed using custom functions written in Matlab (MathWorks). All plots were created using Matlab. Further details on how the tracks were analyzed can be found in the Extended Experimental Procedures.

## SUPPLEMENTAL INFORMATION

Supplemental Information includes Extended Experimental Procedures five figures, two tables, and seven movies and can be found with this article online at http://dx.doi.org/10.1016/j.cell.2013.05.020.

## ACKNOWLEDGMENTS

V.A. carried out all experiments and data analysis. M.S. established a protocol for fast imaging and obtained initial data. S.K.V. performed pilot experiments. A.K. developed the tracking software. I.M.T-N. and N.P. designed the project and wrote the paper with input from V.A. We thank G. Rödel, K. Bloom, K. Sawin, A. Yamashita, and the Yeast Genetic Resource Center for strains and plasmids; Dr. Jacob Kerssemakers and Dr. Marileen Dogterom for the STEPFINDER software; B. Schroth-Diez and D.J. White from the Light Microscopy Facility of MPI-CBG; P. Delivani, D. Ramunno-Johnson, and H. Weisse for technical help; I. Šarić for the drawings; J. Howard, S.W. Grill, N. Maghelli, M. Neetz, M. Chacon, A. Klemm, D. Accardi, and I. Kalinina for discussions and comments on the manuscript; and the Max Planck Society and the German Research Foundation (DFG) for funding.

Received: December 12, 2012
Revised: April 9, 2013
Accepted: May 8, 2013
Published: June 20, 2013

## REFERENCES

Abraham, A.V., Ram, S., Chao, J., Ward, E.S., and Ober, R.J. (2009). Quantitative study of single molecule location estimation techniques. Opt. Express *17*, 23352–23373.

Ali, M.Y., Krementsova, E.B., Kennedy, G.G., Mahaffy, R., Pollard, T.D., Trybus, K.M., and Warshaw, D.M. (2007). Myosin Va maneuvers through actin intersections and diffuses along microtubules. Proc. Natl. Acad. Sci. USA *104*, 4332–4336.

Brouhard, G.J., Stear, J.H., Noetzel, T.L., Al-Bassam, J., Kinoshita, K., Harrison, S.C., Howard, J., and Hyman, A.A. (2008). XMAP215 is a processive microtubule polymerase. Cell *132*, 79–88.

Burakov, A., Nadezhdina, E., Slepchenko, B., and Rodionov, V. (2003). Centrosome positioning in interphase cells. J. Cell Biol. *162*, 963–969.

Cai, D., Verhey, K.J., and Meyhöfer, E. (2007). Tracking single Kinesin molecules in the cytoplasm of mammalian cells. Biophys. J. *92*, 4137–4144.

Carvalho, P., Gupta, M.L., Jr., Hoyt, M.A., and Pellman, D. (2004). Cell cycle control of kinesin-mediated transport of Bik1 (CLIP-170) regulates microtubule stability and dynein activation. Dev. Cell *6*, 815–829.

Chikashige, Y., Ding, D.Q., Funabiki, H., Haraguchi, T., Mashiko, S., Yanagida, M., and Hiraoka, Y. (1994). Telomere-led premeiotic chromosome movement in fission yeast. Science *264*, 270–273.

Coelho, M., Maghelli, N., and Tolić-Nørrelykke, I.M. (2013). Single-molecule imaging in vivo: the dancing building blocks of the cell. Integr. Biol. *5*, 748–758.

Cooper, J.R., and Wordeman, L. (2009). The diffusive interaction of microtubule binding proteins. Curr. Opin. Cell Biol. *21*, 68–73.

Coy, D.L., Hancock, W.O., Wagenbach, M., and Howard, J. (1999). Kinesin's tail domain is an inhibitory regulator of the motor domain. Nat. Cell Biol. *1*, 288–292.

Elowitz, M.B., Surette, M.G., Wolf, P.E., Stock, J.B., and Leibler, S. (1999). Protein mobility in the cytoplasm of Escherichia coli. J. Bacteriol. *181*, 197–203.

English, B.P., Hauryliuk, V., Sanamrad, A., Tankov, S., Dekker, N.H., and Elf, J. (2011). Single-molecule investigations of the stringent response machinery in living bacterial cells. Proc. Natl. Acad. Sci. USA *108*, E365–E373.

Eshel, D., Urrestarazu, L.A., Vissers, S., Jauniaux, J.C., van Vliet-Reedijk, J.C., Planta, R.J., and Gibbons, I.R. (1993). Cytoplasmic dynein is required for normal nuclear segregation in yeast. Proc. Natl. Acad. Sci. USA *90*, 11172–11176.

Forsburg, S.L., and Rhind, N. (2006). Basic methods for fission yeast. Yeast *23*, 173–183.

Friedman, D.S., and Vale, R.D. (1999). Single-molecule analysis of kinesin motility reveals regulation by the cargo-binding tail domain. Nat. Cell Biol. *1*, 293–297.

Gestaut, D.R., Graczyk, B., Cooper, J., Widlund, P.O., Zelter, A., Wordeman, L., Asbury, C.L., and Davis, T.N. (2008). Phosphoregulation and depolymerization-driven movement of the Dam1 complex do not require ring formation. Nat. Cell Biol. *10*, 407–414.

Gönczy, P., Pichler, S., Kirkham, M., and Hyman, A.A. (1999). Cytoplasmic dynein is required for distinct aspects of MTOC positioning, including centrosome separation, in the one cell stage Caenorhabditis elegans embryo. J. Cell Biol. *147*, 135–150.

Hackney, D.D., Levitt, J.D., and Suhan, J. (1992). Kinesin undergoes a 9 S to 6 S conformational transition. J. Biol. Chem. *267*, 8696–8701.

Hammond, J.W., Cai, D., Blasius, T.L., Li, Z., Jiang, Y., Jih, G.T., Meyhofer, E., and Verhey, K.J. (2009). Mammalian Kinesin-3 motors are dimeric in vivo and move by processive motility upon release of autoinhibition. PLoS Biol. *7*, e72.

Hammond, J.W., Blasius, T.L., Soppina, V., Cai, D., and Verhey, K.J. (2010). Autoinhibition of the kinesin-2 motor KIF17 via dual intramolecular mechanisms. J. Cell Biol. *189*, 1013–1025.

Heil-Chapdelaine, R.A., Oberle, J.R., and Cooper, J.A. (2000). The cortical protein Num1p is essential for dynein-dependent interactions of microtubules with the cortex. J. Cell Biol. *151*, 1337–1344.

Helenius, J., Brouhard, G., Kalaidzidis, Y., Diez, S., and Howard, J. (2006). The depolymerizing kinesin MCAK uses lattice diffusion to rapidly target microtubule ends. Nature *441*, 115–119.

Johnson, K.A., and Wall, J.S. (1983). Structure and molecular weight of the dynein ATPase. J. Cell Biol. *96*, 669–678.

Kalinina, I., Nandi, A., Delivani, P., Chacón, M.R., Klemm, A.H., Ramunno-Johnson, D., Krull, A., Lindner, B., Pavin, N., and Tolić-Nørrelykke, I.M. (2013). Pivoting of microtubules around the spindle pole accelerates kinetochore capture. Nat. Cell Biol. *15*, 82–87.

Kapitein, L.C., Janson, M.E., van den Wildenberg, S.M., Hoogenraad, C.C., Schmidt, C.F., and Peterman, E.J. (2008). Microtubule-driven multimerization recruits ase1p onto overlapping microtubules. Curr. Biol. *18*, 1713–1717.

Kimura, K., and Kimura, A. (2011). Intracellular organelles mediate cytoplasmic pulling force for centrosome centration in the Caenorhabditis elegans early embryo. Proc. Natl. Acad. Sci. USA *108*, 137–142.

Krementsov, D.N., Krementsova, E.B., and Trybus, K.M. (2004). Myosin V: regulation by calcium, calmodulin, and the tail domain. J. Cell Biol. *164*, 877–886.

Laan, L., Pavin, N., Husson, J., Romet-Lemonne, G., van Duijn, M., López, M.P., Vale, R.D., Jülicher, F., Reck-Peterson, S.L., and Dogterom, M. (2012). Cortical dynein controls microtubule dynamics to generate pulling forces that position microtubule asters. Cell *148*, 502–514.

Lee, W.L., Oberle, J.R., and Cooper, J.A. (2003). The role of the lissencephaly protein Pac1 during nuclear migration in budding yeast. J. Cell Biol. *160*, 355–364.

Li, Y.Y., Yeh, E., Hays, T., and Bloom, K. (1993). Disruption of mitotic spindle orientation in a yeast dynein mutant. Proc. Natl. Acad. Sci. USA *90*, 10096–10100.

Li, X.D., Mabuchi, K., Ikebe, R., and Ikebe, M. (2004). Ca2+-induced activation of ATPase activity of myosin Va is accompanied with a large conformational change. Biochem. Biophys. Res. Commun. *315*, 538–545.

Mallik, R., Carter, B.C., Lex, S.A., King, S.J., and Gross, S.P. (2004). Cytoplasmic dynein functions as a gear in response to load. Nature *427*, 649–652.

Markus, S.M., and Lee, W.L. (2011). Regulated offloading of cytoplasmic dynein from microtubule plus ends to the cortex. Dev. Cell *20*, 639–651.

Markus, S.M., Punch, J.J., and Lee, W.L. (2009). Motor- and tail-dependent targeting of dynein to microtubule plus ends and the cell cortex. Curr. Biol. *19*, 196–205.

Nguyen-Ngoc, T., Afshar, K., and Gönczy, P. (2007). Coupling of cortical dynein and G alpha proteins mediates spindle positioning in Caenorhabditis elegans. Nat. Cell Biol. *9*, 1294–1302.

O'Connell, C.B., and Wang, Y.L. (2000). Mammalian spindle orientation and position respond to changes in cell shape in a dynein-dependent fashion. Mol. Biol. Cell *11*, 1765–1774.

Palazzo, A.F., Joseph, H.L., Chen, Y.J., Dujardin, D.L., Alberts, A.S., Pfister, K.K., Vallee, R.B., and Gundersen, G.G. (2001). Cdc42, dynein, and dynactin regulate MTOC reorientation independent of Rho-regulated microtubule stabilization. Curr. Biol. *11*, 1536–1541.

Paschal, B.M., and Vallee, R.B. (1987). Retrograde transport by the microtubule-associated protein MAP 1C. Nature *330*, 181–183.

Powers, A.F., Franck, A.D., Gestaut, D.R., Cooper, J., Gracyzk, B., Wei, R.R., Wordeman, L., Davis, T.N., and Asbury, C.L. (2009). The Ndc80 kinetochore complex forms load-bearing attachments to dynamic microtubule tips via biased diffusion. Cell *136*, 865–875.

Reck-Peterson, S.L., Yildiz, A., Carter, A.P., Gennerich, A., Zhang, N., and Vale, R.D. (2006). Single-molecule analysis of dynein processivity and stepping behavior. Cell *126*, 335–348.

Ross, J.L., Wallace, K., Shuman, H., Goldman, Y.E., and Holzbaur, E.L. (2006). Processive bidirectional motion of dynein-dynactin complexes in vitro. Nat. Cell Biol. *8*, 562–570.

Saito, T.T., Okuzaki, D., and Nojima, H. (2006). Mcp5, a meiotic cell cortex protein, is required for nuclear movement mediated by dynein and microtubules in fission yeast. J. Cell Biol. *173*, 27–33.

Schuster, M., Lipowsky, R., Assmann, M.A., Lenz, P., and Steinberg, G. (2011). Transient binding of dynein controls bidirectional long-range motility of early endosomes. Proc. Natl. Acad. Sci. USA *108*, 3618–3623.

Sheeman, B., Carvalho, P., Sagot, I., Geiser, J., Kho, D., Hoyt, M.A., and Pellman, D. (2003). Determinants of S. cerevisiae dynein localization and activation: implications for the mechanism of spindle positioning. Curr. Biol. *13*, 364–372.

Skop, A.R., and White, J.G. (1998). The dynactin complex is required for cleavage plane specification in early Caenorhabditis elegans embryos. Curr. Biol. *8*, 1110–1116.

Toba, S., Watanabe, T.M., Yamaguchi-Okimoto, L., Toyoshima, Y.Y., and Higuchi, H. (2006). Overlapping hand-over-hand mechanism of single molecular motility of cytoplasmic dynein. Proc. Natl. Acad. Sci. USA *103*, 5741–5745.

Tokunaga, M., Imamoto, N., and Sakata-Sogawa, K. (2008). Highly inclined thin illumination enables clear single-molecule imaging in cells. Nat. Methods *5*, 159–161.

Trokter, M., Mücke, N., and Surrey, T. (2012). Reconstitution of the human cytoplasmic dynein complex. Proc. Natl. Acad. Sci. USA *109*, 20895–20900.

Vallee, R.B., Williams, J.C., Varma, D., and Barnhart, L.E. (2004). Dynein: An ancient motor protein involved in multiple modes of transport. J. Neurobiol. *58*, 189–200.

Vogel, S.K., Pavin, N., Maghelli, N., Jülicher, F., and Tolić-Nørrelykke, I.M. (2009). Self-organization of dynein motors generates meiotic nuclear oscillations. PLoS Biol. *7*, e1000087.

Wang, F., Thirumurugan, K., Stafford, W.F., Hammer, J.A., 3rd, Knight, P.J., and Sellers, J.R. (2004). Regulated conformation of myosin V. J. Biol. Chem. *279*, 2333–2336.

Yamamoto, A., West, R.R., McIntosh, J.R., and Hiraoka, Y. (1999). A cytoplasmic dynein heavy chain is required for oscillatory nuclear movement of meiotic prophase and efficient meiotic recombination in fission yeast. J. Cell Biol. *145*, 1233–1249.

Yamamoto, A., Tsutsumi, C., Kojima, H., Oiwa, K., and Hiraoka, Y. (2001). Dynamic behavior of microtubules during dynein-dependent nuclear migrations of meiotic prophase in fission yeast. Mol. Biol. Cell *12*, 3933–3946.

Yamashita, A., and Yamamoto, M. (2006). Fission yeast Num1p is a cortical factor anchoring dynein and is essential for the horse-tail nuclear movement during meiotic prophase. Genetics *173*, 1187–1196.

Yang, F., Moss, L.G., and Phillips, G.N., Jr. (1996). The molecular structure of green fluorescent protein. Nat. Biotechnol. *14*, 1246–1251.